Catalysis Today 141 (2009) 361–366

Contents lists available at ScienceDirect

Catalysis Today

journal homepage: www.elsevier.com/locate/cattod

Total oxidation of toluene on ferrite-type catalysts

M. Florea [a], M. Alifanti [a], V.I. Parvulescu [a,*], D. Mihaila-Tarabasanu [b], L. Diamandescu [b], M. Feder [b], C. Negrila [b], L. Frunza [b]

[a] University of Bucharest, Department of Chemical Technology and Catalysis, Bdul Regina Elisabeta 4-12, 030018 Bucharest, Romania
[b] National Institute of Materials Physics, PO Box MG-07, 077125 Bucharest, Magurele, Romania

ARTICLE INFO

Article history:
Available online 1 July 2008

Keywords:
Toluene oxidation
Ferrites
Hydrothermal preparation

ABSTRACT

Ferrite catalysts were prepared following two routes, i.e. the hydrothermal one and the calcination of an oxide mixture. In the first route sodium hydroxide, ferrous sulfate and the sulfate of the substituting ion (Mn, Ni) were used. The ferrites obtained using this route was $Ni_xFe_{3-x}O_4$ ($x = 0.5$) and $Mn_xFe_{3-x}O_4$ ($x \sim 0.65$). Following the second route were prepared three samples: $NiFe_2O_4$, $Ni_{0.5}Zn_{0.5}Fe_2O_4$ and $MnFe_2O_4$. Two of them contain the corresponding ferrites while the latter is a presintered oxide mixture (Fe_2O_3–Mn_2O_3). All the samples were fully characterized using chemical analysis, X-ray fluorescence spectroscopy and EDX, nitrogen adsorption–desorption isotherms at −196 °C, X-ray diffraction (XRD), FTIR, scanning electron microscopy and XPS. The catalytic activity evaluation was made using a mixture of 1700 ppm vol. of toluene and air flowing at 100 ml min^{-1} raising the temperature up to 600 °C in steps of 25 °C. Among these systems the sample representing the presintered Fe_2O_3–Mn_2O_3 mixture showed the highest activity.

1. Introduction

The synthesis of nanosize-structured spinel ferrites [1,2] was already reported to provide selective catalysts for oxidation of hydrocarbons. These materials were found to be very good catalysts for the oxidation of styrene to benzaldehyde in the presence of hydrogen peroxide [3,4]. More complex structures are able to activate very stable molecules as methane [5]. The reactivity and mobility of the surface and lattice oxygen in a $La_{1-x}Ca_xFeO_{3-y}$ catalyst system was reported to depend on the reaction temperature. While for middle-temperatures (400–700 °C) oxygen lattice mobility reaches maximum for samples with disordered anion vacancies, at high temperatures the lattice oxygen flux appears to be controlled by a rapid transfer along disordered domain walls [5]. In the high-temperature range, a high selectivity to syngas of methane oxidated by the lattice oxygen was achieved both for pure lanthanum ferrite and for samples with a microdomain individual oxide structure.

Catalysts exhibiting mobile surface and lattice oxygen were also tested in total oxidation of toluene. The compositional flexibility of perovskites induces interesting and useful properties. The base formulations used for total oxidation reactions include Fe, Co, Ni and Mn at B-site and La (as well or partially substituted by other lanthanide or alkaline earth metals) at A-site. The addition of a noble metal to the above perovskites was found to even increase the catalytic performances for total oxidation of aromatic hydrocarbons [6]. Thus, calcined and reduced catalysts $Pd/LaBO_3$ (B═Co, Fe, Mn and Ni) were used for the total oxidation of toluene [6]. Under reaction conditions both Pd and B species were found to coexist in different valence levels by creating complex surface redox states. However, among the different perovskites only $LaFeO_3$ was able to preserve the dispersion of palladium.

Since the major drawback of using perovskites for catalytic purposes is the low surface area their deposition or embedding on adequate refractory supports was reported as a suitable route for solving these problems [7–10]. Among the different carriers, ceria-based materials and zirconia were reported as good supports, leading to no interaction with the most common cations of perovskites [11–13]. Toluene oxidation on such structures occurred with high conversions for relatively low temperatures and high space velocities [14,15].

Other reported catalysts for total oxidation of toluene are mixed $Co_2Mn_4Al_2$ oxides with high specific surface areas prepared via thermal decomposition of hydrotalcites. These catalysts contain in fact a mixing of nano-crystallites of Co-spinel, Mn_5O_8 and $CoMnO_3$ phases that exhibit redox properties [16].

Based on this background the aim of this study was to investigate the behavior of another oxidic structure, namely, ferrites in total oxidation of toluene. For such a purpose we prepared nickel- and manganese-based ferrites using two different

* Corresponding author. Tel.: +40 21 4100241; fax: +40 21 4100241.
E-mail address: v_parvulescu@chem.unibuc.ro (V.I. Parvulescu).

0920-5861/$ – see front matter © 2008 Elsevier B.V. All rights reserved.
doi:10.1016/j.cattod.2008.05.005

pathways (hydrothermally and oxide calcination). The selection of nickel, manganese and iron was based on the performances of these components in total oxidation by using perovskites. Different characterization techniques were applied in order to check the oxygen lattice mobility.

2. Experimental

The catalysts were prepared by following two routes, i.e. the hydrothermal one and the calcination of an oxide mixture. Ferrites F1 and F2 (Table 1) were prepared via a hydrothermal route, already described [1,2]. Natrium hydroxide, ferrous sulfate and the sulfate of the substituting ion (Mn, Ni) (Merck analytical grade reagents) were introduced in a stainless steel autoclave and stirred at 200 °C for 2 h. The heating rate was of 4 °C/min. The pH of the solutions was adjusted to ensure the complete precipitation of the metal ions. After 2 h, the autoclave was cooled at room temperature and the black precipitate was filtered, washed and dried in air at 110 °C and calcined at 600 °C.

In the second procedure, samples F3–F5 were prepared by calcination of the appropriate oxide mixture, using a conventional ceramic procedure [5,17]. The syntheses started from Merck purity materials: α-Fe_2O_3 (containing 99.3 wt% Fe_2O_3); $NiCO_3{\cdot}Ni(OH)_2{\cdot}H_2O$ (containing 60.0 wt% NiO), ZnO (containing 99.2 wt% ZnO), and Mn_3O_4 (91.4 wt% MnO) which were mixed in suitable proportions in a steel ball mill, using demineralized water as a dispersion medium. The resulted material was dried in air at 110 °C and the resulted powder was then calcinated at 850 °C for 3 h. Then the materials were milled for 8 h in a steel ball mill. Table 1 compiles the chemical formula of the resulted samples and their morphology.

All the samples were fully characterized by X-ray diffraction (XRD) (using both a Siefert equipment and a Rigaku D-2013 diffractometer with Cu Kα radiation in the range 20–70 2θ), XPS (with a VG ESCA 3 Mk II spectrometer with Al Kα radiation; energy calibration used the C 1s binding energy (284.8 eV); Shirley type background was subtracted for spectra decomposition into Voigt profiles; the broadening was of 1.8 eV (50 V pass energy of the analyzer)), IR (KBr technique, Spectrum BX FTIR apparatus, 200 scans for each measurement), and by nitrogen adsorption–desorption isotherms at −196 °C (Micromeritics ASAP 2000) after out-gassing the samples at 120 °C for 12 h. The cation concentration was determined by X-ray fluorescence spectroscopy and EDX [1,2]. SEM and EDX measurements were performed on a Hitachi S3000N scanning electron microscope, equipped with a Horiba electron microprobe. Thermal analysis experiments were carried out using SETARAM TG DTA 92 apparatus. The heating rate was kept at 10 °C/min from room temperature to 1100 °C. The mass of solid specimen was about 20 mg in each run. The measurements were performed in dry air (50 ml/min).

For catalytic activity evaluation, a mixture of 1700 ppm vol. of toluene and air flowing at 100 ml min^{-1} (total GHSV = 60,000 ml g^{-1} cat h^{-1}) was admitted and the temperature was raised up to 600 °C in steps of 25 °C. The CO_2 level in the outlet was continuously monitored by means of an on-line coupled IR-Fisher-Rosemount multichannel analyzer while the CO production was on-line checked by an IAQ CALC-METER model 8762 from COLE-PARMER. Hydrocarbons and byproducts were analyzed using a Porapaq Q column mounted on a HP 5890 Series II GC equipped with a TCD detector. During catalytic runs, temperature was increased to a superior value only after reaching a steady level of CO_2 in the outlet (typically after 25–30 min). Conversion levels at decreasing temperature superposed on the levels at increasing temperature. Each catalytic run was performed twice, considering only the results for which the differences between two sets of results were below 10%. Carbon balance closed for all investigated materials and the analysis of spent catalysts did not show any carbonaceous deposits at the surface.

3. Results and discussion

3.1. Catalysts characterization

The X-ray diffraction patterns of the F1 and F2 samples indicate that both hydrothermally obtained ferrites have the majority phase belonging to the cubic spinel magnetite structure (see Fig. 1). In the XRD patterns of F2 sample a small amount of α-Fe (∼1%) is present as a result of reduction phenomena in the hydrothermal. Polyhedral particles with uniform dimensional distribution and submicron size were obtained (Table 1 and Fig. 2), but their cation concentration as determined by X-ray fluorescence spectroscopy [1,2] was smaller than that at synthesis stage. The apparent greater line width for F2 in comparison with F1 is a scale effect.

The X-ray diffraction patterns for the samples obtained by classical ceramic procedure show diffraction peaks specific for spinellic phase but in addition peaks for the un-transformed precursors like α-Fe_2O_3, NiO, ZnO and Mn_2O_3 (Fig. 1b). In particular, in the case of F5 sample the ferritisation process was not confirmed and the XRD pattern is represented by a mixture of α-Fe_2O_3 and Mn_2O_3, as revealed by the Rietveld refinement (Table 1). Beside the phase composition the Rietveld analysis has also provided particle size (Table 1). Micropicture in Fig. 2 stands for a rather uniform structure with grain dimension ranging in a micrometer domain. The porosity of the sample is rather high due to the soft sintering conditions. A very similar image was resulted for the sample F1 as well.

Table 1
Phase composition and particle size for the investigated samples

Sample label	Composition at synthesis stage	Preparing method	Phase composition (from XRD)	Particle size (from XRD) (nm)
F1	$Ni_xFe_{3-x}O_4$ ($x = 0.5$)	Hydrothermally	$Ni_xFe_{3-x}O_4$ ($x = 0.5$), 100%	90
F2	$Mn_xFe_{3-x}O_4$ ($x \sim 0.65$)	Hydrothermally	$Mn_xFe_{3-x}O_4$ ($x \sim 0.65$), 98.6% α-Fe 1.4%	180 60
F3	$NiFe_2O_4$	Oxide calcination	$NiFe_2O_4$, 20.5% α-Fe_2O_3, 61.3% NiO, 18.2%	55 88 56
F4	$Ni_{0.5}Zn_{0.5}Fe_2O_4$	Oxide calcination	$Ni_{0.5}Zn_{0.5}Fe_2O_4$, 46.6% α-Fe_2O_3, 41.3% NiO, 9.7% ZnO, 2.4%	48 87 45 86
F5	$MnFe_2O_4$	Oxide calcination	α-Fe_2O_3, 67.4% Mn_2O_3, 32.6%	42 68

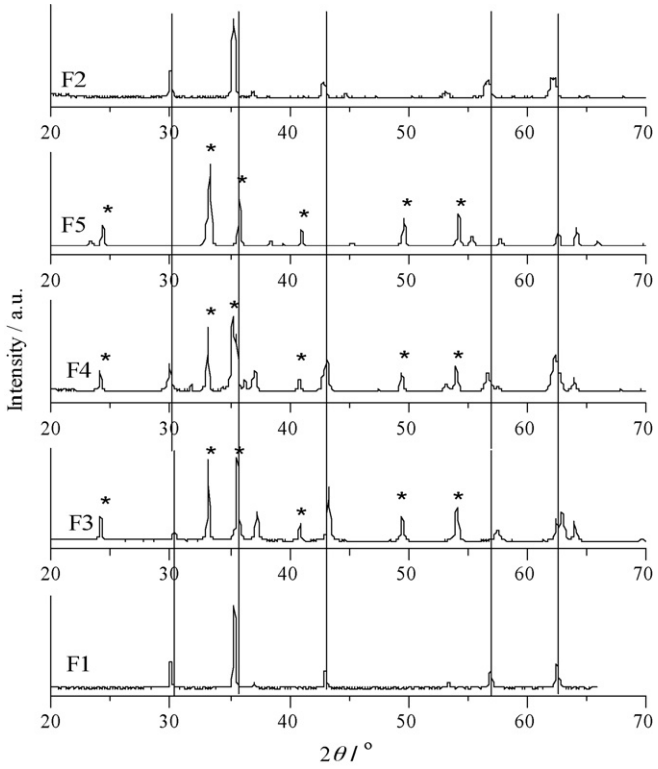

Fig. 1. XRD patterns of the investigated samples. The vertical lines show the main ferrite peaks. The stars indicate the peaks of α-Fe_2O_3.

Textural characterization of these samples showed that the pathway of the preparation has an influence on the surface area. While F1 and F2 exhibit surface areas around 15 $m^2\,g^{-1}$ (F1 14.7 $m^2\,g^{-1}$ and F2 15.4 $m^2\,g^{-1}$, respectively), the samples prepared via calcination have surface areas almost five times smaller (F3 2.9 $m^2\,g^{-1}$, F4 2.8 $m^2\,g^{-1}$ and F5 3.1 $m^2\,g^{-1}$).

Thermal analysis of the investigated samples after these have been calcined showed a different behavior. Thus, in the range 250–550 °C, the mass of F1 and F2 samples increases and, as confirmed by XPS, this was due to the sample oxidation. However, this increase is very small (of the order of 2 wt%). Fig. 3 shows typical TG, heat flow and DTG curves for these samples. Heating at higher temperatures results in a small mass decrease. To prove this effect, these samples were re-heated at 600 °C and re-analyzed using TG, DTG and heat flow curves. Repeating this experiment three times they were obtained perfectly reproducible results, suggesting that at temperatures higher than 550 °C some oxygen is released and this can be recovered by heating below this temperature. The behavior of the other three samples F3–F5 was different. These lose some mass (less than 0.5 wt%) during heating till 200 °C, most probably due to the adsorption of a few water molecules onto the sample or due to oxygen adsorption during manipulation. The heat flow corresponds to an exothermic effect that is a proof of the chemisorption of these species. Increasing the temperature in the range 200–600 °C was not accompanied by any thermal effect (changes in the mass loss or any heat flow effect). To confirm this behavior, the experiment was repeated three times without removing the sample from the apparatus. In the repeated experiments, no mass change and no heat flow effects have been detected, confirming the supposition of the adventitious chemisorption of water or oxygen molecules.

Table 2 compiles the binding energies assigned to 2p level in the investigated samples. The transition metal ions were corresponding $2p_{1/2}$ and $2p_{3/2}$ photoelectron levels. In this aim, the Scofield

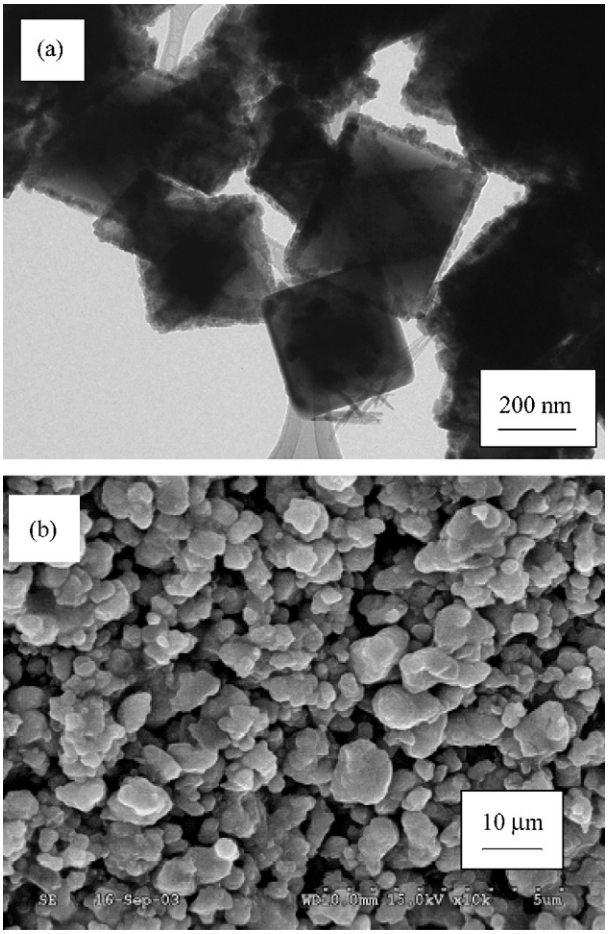

Fig. 2. SEM micrograph for the investigated samples F2 (a) and F4 (b).

factor of the equipment software was used by referring to C 1s factor taken as 1.

For the case of iron, it was already reported that the Fe 2p photoelectron peaks associated to oxidized iron species exhibit satellite peaks [18–20]. In principle, the satellite peak is generated by the photoemission of the oxide Fe site. The relaxation is accompanied by a significant charge transfer in the valance band of Fe^{x+} sites from the ligand (oxygen). As the Fe^{2+} and Fe^{3+} states

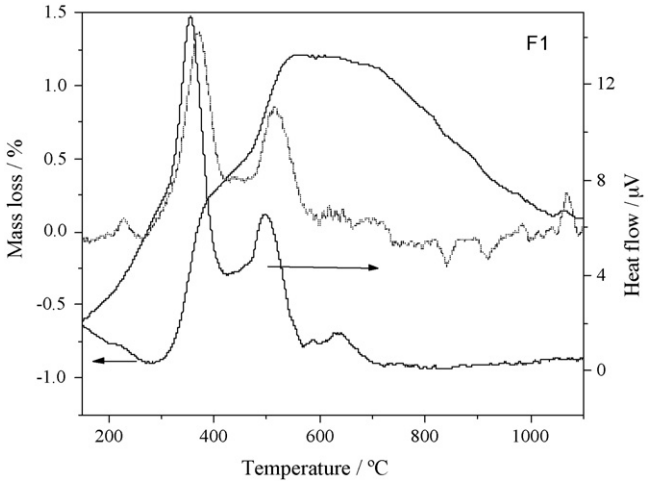

Fig. 3. TG, DTG and heat flow curves for the sample F1. Dotted line indicates DTG curve.

Table 2
Binding energies (eV) assigned to 2p level in the investigated samples

Sample	Binding energy (eV)				
	Fe $2p_{3/2}$		Ni $2p_{3/2}$	Mn $2p_{3/2}$	Zn $2p_{3/2}$
F1	710.75	17.84	855.7		
F2	710.90	19.12		641.20	
F3	710.88	19.27	854.63		
F4	711.03	19.32	855.52		1021
F5	710.78	19.03		641.63	

correspond to d^6 and d^5, respectively, the satellite peak is located at different energies representing a characteristic of the oxidation state of iron. The Fe^{2+} $2p_{3/2}$ peak at ca. 709.5 eV is always associated with a satellite peak at 6.0 eV above the principal peak, while the Fe^{3+} $2p_{3/2}$ peak at ca. 711 eV is associated with a satellite peak at 8.0 eV above [20]. Depending on the surrounding, the $2p_{3/2}$ peaks of ferrites might have different positions but the presence of satellites at 8–9 eV above the main peak is a clear indication of the absence of Fe^{2+} species [21]. Having this background, the data compiled in Table 2 sustain the fact that iron is mostly oxidized at Fe^{3+} state in the investigated F1–F5 samples. However, F1 shows the lowest position of the $2p_{3/2}$ peak but the largest halfwidth, meaning that some Fe^{2+} species might be still present. The $2p_{3/2}$ peak is the most shifted in the case of F2, meaning that the iron is more oxidized than in the other samples.

For the case of nickel, the Ni $2p_{3/2}$ peak of $NiFe_2O_4$ was generally observed around 855 eV. Although XRD evidenced the formation of NiO in F3 and F4 samples, from the deconvolution of the Ni $2p_{3/2}$ peak it is hard to assign the existence of these species. However, satellite peaks due to shake-up processes [22,23] were evidenced for all the analyzed samples in the range 860–865 eV as it can be seen from the same (Table 2).

Binding energy of the $Mn2p_{3/2}$ level corresponds to Mn^{3+} species [24] as XRD analysis indicates the formation of Mn_2O_3. Both XPS and XRD supplied no evidence of the formation of MnO_2 species. The binding energy of the Zn $2p_{3/2}$ level is typical for Zn^{2+} species [25,26].

Table 3 presents the comparative XPS surface and analytic bulk composition. This comparison shows again clear differences between F1 and F2, and F3–F5 ones. The surface of samples F1 and F2 is more enriched in iron than that of the samples F3–F5. However, for all the samples the surface iron content is inferior to the bulk one. The situation is different for the second or the third element. The surface content for Ni, Zn and even Mn is higher than the bulk one, but differences among the two kinds of samples are less evident.

The IR spectra collected at room temperature in the range 1000–400 cm^{-1} for all the samples show two of the fundamental absorption bands ν_1 (601–549 cm^{-1}, due to stretching vibration of tetrahedral groups FeO_4) and ν_2 (512–406 cm^{-1} due to stretching vibration of octahedral groups FeO_6) [27–29]. The splitting of the band ν_2 is generally related to the nature of the octahedral site in the ferrite [30] since in our particular case other factors of importance like the radius and the atomic mass of the metal ions

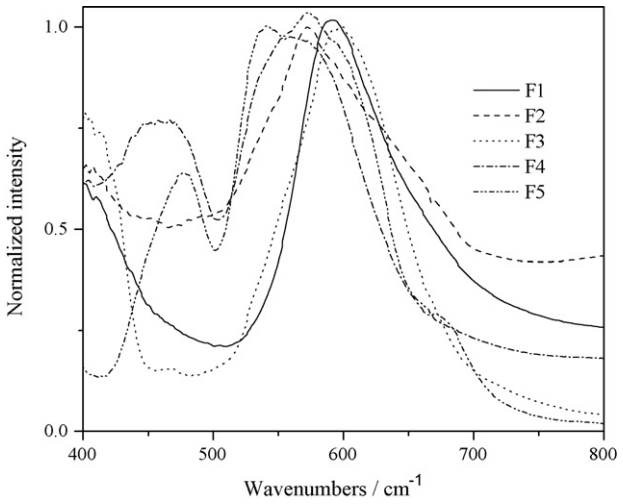

Fig. 4. FTIR spectra of the investigated samples.

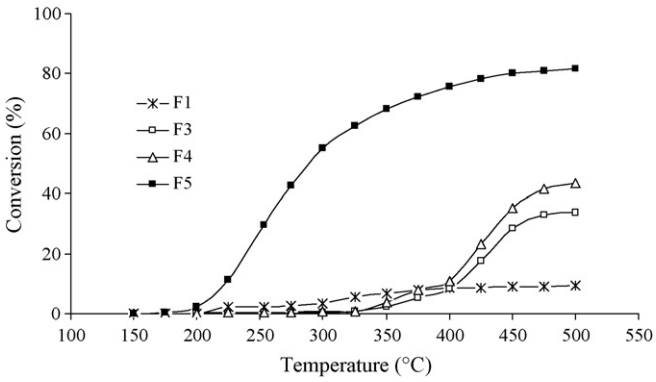

Fig. 5. Time-on-stream dependence of the conversion with temperature in total oxidation of toluene.

are quite similar. Fig. 4 shows again differences between hydrothermal synthesized catalysts and those prepared via calcination of mixed oxides. The sample F5 shows strong bands at approximately 470 and 540 cm^{-1}, characteristic of well-crystallized hematite [31,32] while NiO in the samples F3 and F4 gives a broad band at approximately 466–470 cm^{-1} [33] overlapping that of hematite present as well in these samples. Since the particles which form the samples have nanometric size, the bands belonging to the internal modes might be additionally splitted due to surface phonon modes at least in the case of MnO_6 groups [34].

3.2. Catalytic behavior

Fig. 5 shows the evolution of the conversion with temperature. The inflexion temperatures of the light-off curves paralleled with the conversion. The results obtained using $Ni_xFe_{3-x}O_4$ ($x = 0.5$)

Table 3
Comparative XPS surface and analytic bulk composition (% atoms without considering surface C)

Sample	O surface/bulk[a]	Fe surface/bulk	Ni surface/bulk	Mn surface/bulk	Zn surface/bulk
F1	69/57	14/36	17/7.0	0	0
F2	65/57	13/28	0	22/9	0
F3	78/57	5/34	17/7.5	0	0
F4	61/57	7/28	13/7.5	0	19/7.5
F5	73/54	9/28	0	18/15	0

[a] Theoretical, at synthesis.

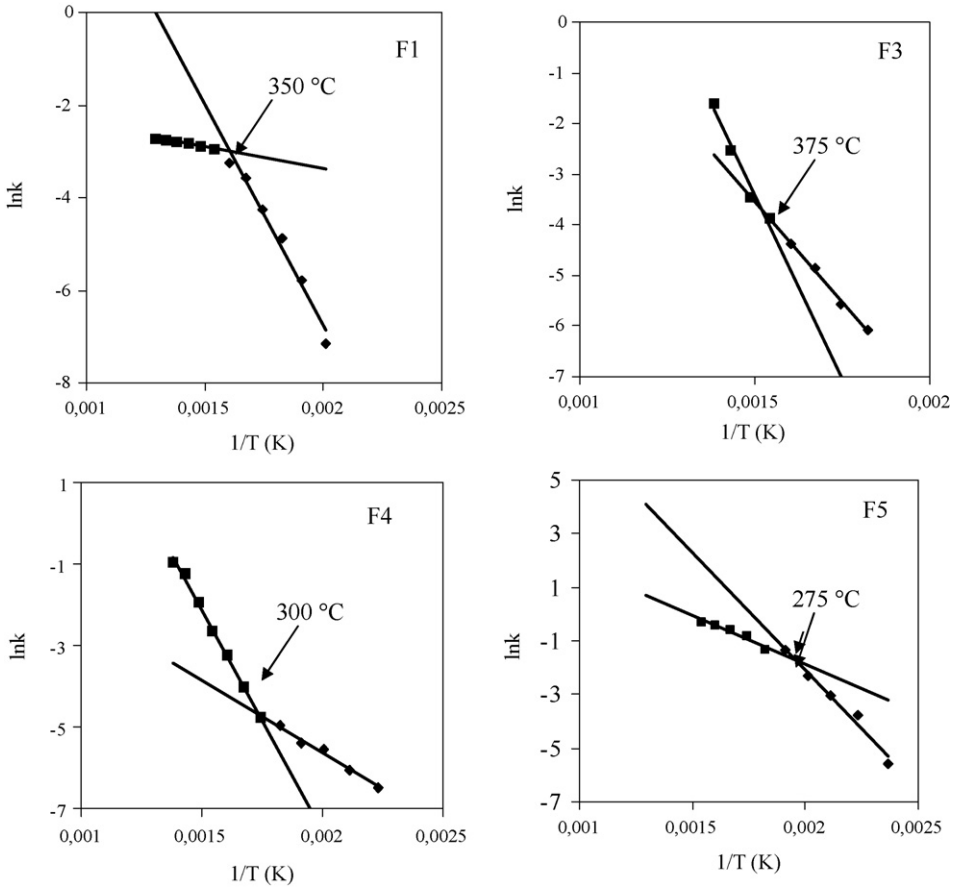

Fig. 6. Arrhenius plots for total oxidation of toluene on the investigated ferrites.

were very similar with those obtained using $Mn_xFe_{3-x}O_4$ ($x \sim 0.65$), and therefore the last ones were not included in the figure. These data show that well-structured ferrites obtained using the hydrothermal pathway exhibit a very low activity in total oxidation of toluene. The most active system in this reaction was the sample F5 on which conversions higher than 80% were obtained at around 500 °C. However, the comparison of the sample F5 with F3 shows a different activity of the intimate mixed oxides. Manganese oxide in combination with iron oxide is leading to a more active system than those resulted from nickel and iron oxides.

In all the outlet streams only unreacted hydrocarbons, CO_2 and water were detected. In the temperature range of our experiments no thermal destruction of the oxidized molecules has been detected.

Since XRD measurements showed large amounts of non-reacted MnO and Fe_2O_3, in order to assign the catalytic activity, we prepared a physical mixture of α-Fe_2O_3 (88.5%) and MnO (11.5%) that after 2 h milling was exposed to the catalytic reaction. The physical mixture behaved as bad as the hydrothermally prepared samples. We have also tested a mixture of the ferrite F2 and α-Fe_2O_3 and MnO in appropriate ratios with those given by the pattern F5 in Fig. 1, but the results were similar with that obtained using only the mixture of two oxides. Under these conditions it is logical to suppose that the catalytic activity of this system should be assigned to an intrinsic interaction between the phases that cannot be achieved by a simple mixing. Although the addition of Zn in the sample F4 led to a slight increase of the conversion compared with F3, but the activity of these ferrites is quite poor by comparing with F5.

Actually, these data correlate very well with the structural characterization obtained by XRD and XPS spectroscopy, and with thermal analysis data. F1 and F2 till pretty high temperatures exhibit the tendency to be oxidized themselves, while the others have a quite complex structure of oxides that generates catalytic activity. TG analysis has shown that F1 and F2 samples, starting from 120 °C increase their weight due to an oxygen capture. As a consequence, their cations especially from the octahedral sites are oxidized. The other ferrites lose some weight during calcination, probably that resulting from OH groups or from surface species.

Fig. 6 gives the Arrhenius plots for total oxidation of toluene on the investigated ferrites and Table 4 the corresponding activation energies. A better image on the activity of the different ferrites phase can be obtained expressing the catalytic activity in terms of reaction rates. The results expressed per mass unit of ferrite were obtained assuming a first order kinetics with respect to toluene and zero order for oxygen, in a plug-flow reactor [35]. The treatment of the experimental data using this approach showed, as it can be seen from Fig. 6, two domains: one below 370 °C dominated by a kinetic regime, and another at higher tempera-

Table 4
The activation energies for total oxidation of toluene on the investigated ferrites

Sample	Activation energy (kcal/mol)	
	Step 1	Step 2
F1	8.0	79.8
F3	50.9	76.8
F4	29.5	88.7
F5	11.1	73.1

tures, dominated by a mass transfer and equilibrium regime. The temperature at which the process passes from a regime to another is well correlated with the catalytic activity. On the other side, it is clear that there is no deactivation of the catalysts, and that the values given for the step 2 cannot be associate with such a process. Cooling the reactor with the same rate led to the conversions identical with those give in Fig. 5.

The very small values of the activation energy for the samples F1 and F5 in the first step indicate the dominant contribution of the mass transfer effects. Therefore, for these catalysts the kinetic data we have determined do not offer criteria to differentiate the two catalysts. But, for the catalyst F3 the very high activation energy in the first step offers a clear explanation of the small activity of this catalyst.

4. Conclusions

Ferrite-type catalysts may constitute an alternative for perovskites for total oxidation of hydrocarbons. The structure of the catalysts is very important in providing catalytic active structures. Pure XRD ferrite structures exhibit a poor activity, while mixed-phase ferrite-oxide showed a good activity. The activity of the mixed-phase ferrite-oxide should be ascribed to an intimate interaction, since the physical mixture of ferrites with the corresponding oxides resulted in very poor catalysts.

Acknowledgements

Financial support from Romanian Ministry of Education and Research under CNCSIS, CEEX C25 and CERES 4-81 Projects is gratefully acknowledged. Measurements performed in ACA-Berlin under EU-funded Coordination Action CONCORDE Project and in NIMP by Dr. C. Ghica are highly appreciated.

References

[1] L. Diamandescu, D. Mihaila-Tarabasanu, V. Teodorescu, N. Popescu-Pogrion, Mater. Lett. 37 (1998) 340–348.
[2] M. Sorescu, L. Diamandescu, R.A. Brand, D. Tarabasanu-Mihaila, Mater. Lett. 58 (2004) 885–888.
[3] D. Guin, B. Baruwati, S.V. Manorama, J. Mol. Catal. A: Chem. 242 (2005) 26–31.
[4] R. Ramanathan, S. Sugunan, Catal. Commun. 8 (2007) 1521–1526.
[5] O. Caltun, M. Feder, C.J. Liu, J. Optoelectr. Adv. Mater. 6 (2004) 955–958.
[6] J.-M. Giraudon, A. Elhachimi, F. Wyrwalski, S. Siffert, A. Aboukaı, Appl. Catal. B: Environ. 75 (2007) 157–166.
[7] P.O. Thevenin, A.G. Ersson, H.M. Kusar, P.G. Menon, S.G. Jaras, Appl. Catal. A: Gen. 212 (2001) 189–197.
[8] D. Klvana, J. Kirchnerova, J. Chaouki, J. Delval, W. Yaici, Catal. Today 47 (1999) 115–121.
[9] R. Schneider, D. Kiessling, G. Wendt, W. Burckhardt, G. Winterstein, Catal. Today 47 (1999) 429–435.
[10] S.D. Peter, E. Garbowski, V. Perrichon, M. Primet, Catal. Lett. 70 (2000) 27–33.
[11] S. Colonna, D. De Rossi, M. Faticanti, I. Pettiti, P. Porta, J. Mol. Catal. A: Chem. 187 (2002) 269–276.
[12] S. Cimino, S. Colonna, S. De Rossi, M. Faticanti, L. Lisi, I. Pettiti, P. Porta, J. Catal. 205 (2002) 309–317.
[13] M. Alifanti, N. Blangenois, M. Florea, B. Delmon, Appl. Catal. A: Gen. 280 (2005) 255–265.
[14] M. Alifanti, M. Florea, S. Somacescu, V.I. Parvulescu, Appl. Catal. B: Environ. 60 (2005) 33–39.
[15] M. Alifanti, M. Florea, G. Filotti, V. Kuncser, V. Cortes-Corberan, V.I. Parvulescu, Catal. Today 117 (2006) 329–336.
[16] J.-F. Lamonier, A.-B. Boutoundou, C. Gennequin, M.J. Perez-Zurita, S. Siffert, A. Aboukais, Catal. Lett. 118 (2007) 165–172.
[17] M. Sorescu, L. Diamandescu, R. Swaminathan, M.E. McHenry, M. Feder, J. Appl. Phys. 97 (2005) 100–105.
[18] T. Schedel-Niedrig, W. Weiss, R. Schlogl, Phys. Rev. B 52 (1995) 17449–17453.
[19] L. Pan, G. Zhang, C. Fan, H. Qiu, P. Wu, F. Wang, Y. Zhang, Thin Solid Films 473 (2005) 63–67.
[20] C. Wandelt, Surf. Sci. Rep. 2 (1982) 1–10.
[21] K. Mittal, P. Chandramohan, S. Bera, M.P. Srinivasan, S. Velmurugan, S.V. Narasimhan, Solid State Commun. 137 (2006) 6–10.
[22] K.S. Kim, N. Winograd, Surf. Sci. 43 (1974) 625–643.
[23] M. Chigane, M. Ishikawa, J. Chem. Soc., Faraday Trans. 94 (1998) 3665–3670.
[24] C.E. Deshpande, S. Badrinarayanan, S.K. Date, J. Mater. Sci. Lett. 4 (1985) 922–924.
[25] H. Kaneko, N. Kojima, N. Hasegawa, M. Inoue, R. Uehara, N. Gokon, Y. Tamaura, T. Sanob, Int. J. Hydrogen Energy 27 (2002) 1023–1028.
[26] M. Sorescu, L. Diamandescu, J. Wood, J. Phys. Chem. Solids 68 (2007) 426–430.
[27] R.D. Waldron, Phys. Rev. 99 (1955) 1727–1735.
[28] P. Tarte, J. Preudhomme, Acta Crystallogr. 16 (1963) 227–234.
[29] J. Preudhomme, P. Tarte, Spectrochim. Acta 27A (1971) 961–965.
[30] L.M. Salah, Phys. Status Solid 271 (2006) 203–207.
[31] Sh. Yariv, E. Mendelovici, Appl. Spectrosc. 33 (1979) 410–411.
[32] A.A. Kamneva, M. Ristic, J. Mol. Struct. 408/409 (1997) 301–304.
[33] S. Music, S. Popovic, S. Dalipi, J. Mater. Sci. 28 (1993) 1793–1798.
[34] L. Zheng, K. Li, Y. Zhang, Phys. Rev. B 58 (1998) 8613–8616.
[35] M. Alifanti, M. Florea, V.I. Parvulescu, Appl. Catal. B: Environ. 70 (2007) 400–405.